



*Supplement of*

## **Chlorine-initiated oxidation of *n*-alkanes under high-NO<sub>x</sub> conditions: insights into secondary organic aerosol composition and volatility using a FIGAERO-CIMS**

**Dongyu S. Wang and Lea Hildebrandt Ruiz**

*Correspondence to:* Lea Hildebrandt Ruiz (lhr@che.utexas.edu)

The copyright of individual parts of the supplement might differ from the CC BY 4.0 License.

## S1 Additional Table and Figures

**Table S1. SOA Bulk Composition and Alternative Yields**

Exp #	Precursors	RH	Y <sub>SOA</sub> <sup>a</sup>	MW <sup>b</sup>	Y <sub>SOA,m</sub> <sup>c</sup>	ρ <sup>d</sup>	Y <sub>SOA,L</sub> <sup>e</sup>	f <sub>HClA</sub> <sup>f</sup>	f <sub>ClF</sub> <sup>g</sup>	f <sub>OCl</sub> <sup>h</sup>	f <sub>ON</sub> <sup>i</sup>	R <sub>ON</sub> <sup>j</sup>
1	Octane, NO, Cl <sub>2</sub>	5 >	0.28	226	0.14	2.3	0.13	1.3 E <sup>-2</sup>	1.8 E <sup>-2</sup>	0.15	0.54	0.64
2	Octane, NO <sub>2</sub> , Cl <sub>2</sub>	5 >	0.16	223	0.08	1.7	0.10	1.1 E <sup>-2</sup>	1.7 E <sup>-2</sup>	0.14	0.49	0.57
3	Octane, NO, NO <sub>2</sub> , Cl <sub>2</sub>	5 >	0.24	206	0.13	1.8	0.14	1.0 E <sup>-2</sup>	2.1 E <sup>-2</sup>	0.15	0.49	0.57
4	Octane, NO, NO <sub>2</sub> , Cl <sub>2</sub>	35	0.24	223	0.12	2.1	0.12	1.4 E <sup>-2</sup>	1.9 E <sup>-2</sup>	0.14	0.49	0.57
5	Decane, NO, Cl <sub>2</sub>	5 >	0.84	265	0.45	2.3	0.39	1.1 E <sup>-2</sup>	1.5 E <sup>-2</sup>	0.13	0.60	0.84
6	Decane, NO <sub>2</sub> , Cl <sub>2</sub>	5 >	0.45	249	0.26	2.0	0.24	1.0 E <sup>-2</sup>	1.6 E <sup>-2</sup>	0.14	0.56	0.75
7	Decane, NO, NO <sub>2</sub> , Cl <sub>2</sub>	5 >	0.80	241	0.47	2.1	0.40	1.2 E <sup>-2</sup>	1.6 E <sup>-2</sup>	0.12	0.59	0.75
8	Decane, NO, NO <sub>2</sub> , Cl <sub>2</sub>	40	0.50	243	0.29	1.6	0.33	1.2 E <sup>-2</sup>	1.7 E <sup>-2</sup>	0.13	0.56	0.71
9	Dodecane, NO, Cl <sub>2</sub>	5 >	1.65	270	1.04	1.8	0.99	0.8 E <sup>-2</sup>	1.7 E <sup>-2</sup>	0.14	0.67	0.93
10	Dodecane, NO <sub>2</sub> , Cl <sub>2</sub>	5 >	1.25	258	0.82	2.1	0.63	1.4 E <sup>-2</sup>	1.7 E <sup>-2</sup>	0.14	0.60	0.78
11	Dodecane, NO, NO <sub>2</sub> , Cl <sub>2</sub>	5 >	1.40	264	0.90	2.4	0.62	1.4 E <sup>-2</sup>	1.8 E <sup>-2</sup>	0.15	0.62	0.82
12	Dodecane, NO, NO <sub>2</sub> , Cl <sub>2</sub>	67	1.10	260	0.72	2.4	0.49	1.1 E <sup>-2</sup>	1.6 E <sup>-2</sup>	0.13	0.61	0.77

- (a) Assuming a CE of 0.5 and RIE of 1.4 for ACSM, in  $\mu\text{g m}^{-3}$
- 5 (b) Average molecular weight calculated based on organic ions (I<sup>-</sup> adducts only) observed by FIGAERO-CIMS in  $\text{g mol}^{-1}$
- (c) SOA molar yield, calculated using Eqs. S1-3, in  $\text{mol mol}^{-1}$
- (d) Density calculated based ACSM mass measurements and SEMS volume measurements
- (e) SOA mass yield, recalculated assuming the lowest reported alkane-OH density,  $1.06 \text{ g cm}^{-3}$  (Lim and Ziemann, 2009), in  $\mu\text{g m}^{-3}$
- 10 (f) Mass fraction of -Cl functional group, estimated using the ACSM measurement of HCl<sup>+</sup> ion, relative to the bulk SOA
- (g) Mass fraction of -Cl functional group, estimated using the SOA molecular composition as measured by the FIGAERO-CIMS, relative to the total organic ions observed
- (h) Mass fraction of organochlorides (including chloronitrates), estimated using the SOA molecular composition as measured by the FIGAERO-CIMS, relative to the total organic ions observed
- 15 (i) Mass fraction of organonitrates (excluding chloronitrates), estimated using the SOA molecular composition as measured by the FIGAERO-CIMS, relative to the total organic ions observed
- (j) Average ratio of -NO<sub>3</sub> functional group to the number of carbon, estimated using the SOA molecular composition as measured by the FIGAERO-CIMS. Individual -NO<sub>3</sub> functional groups in dinitrates and trinitrates are counted separately (e.g. a C<sub>12</sub> dinitrate has the same R<sub>ON</sub> as a C<sub>6</sub> mononitrate).

20

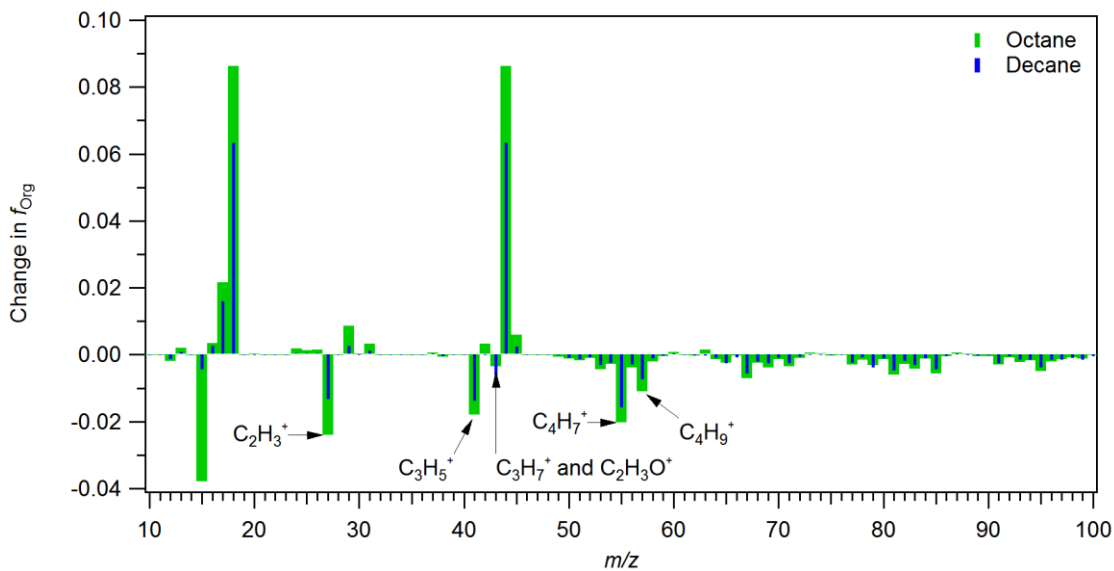


**Figure S1:** Change in the fractional contribution by different organic ion fragments to the overall organic aerosol mass as measured by the ACSM. Dodecane-Cl SOA (Exp. 11) was used as the reference for octane-Cl SOA (Exp. 3) and decane-Cl SOA (Exp. 7) produced under similar oxidation conditions under low RH. Mass spectra shown are 50-minute averages from minute 10 to 60 during the photooxidation period. Ion identities indicated (C<sub>2</sub>H<sub>3</sub><sup>+</sup>, C<sub>3</sub>H<sub>5</sub><sup>+</sup>, C<sub>3</sub>H<sub>7</sub><sup>+</sup>, C<sub>2</sub>H<sub>3</sub>O<sup>+</sup>, C<sub>4</sub>H<sub>7</sub><sup>+</sup>, C<sub>4</sub>H<sub>9</sub><sup>+</sup>) were assumed, as the quadruple ACSM used lacks the necessary mass resolution for exact identification. At  $m/z$  43, the C<sub>2</sub>H<sub>3</sub>O<sup>+</sup> is expected to dominate. Highlighted C<sub>x</sub>H<sub>y</sub> ions are often associated with hydrocarbon-like organic aerosol (Ng et al., 2011; Ulbrich et al., 2009). Clear enhancement of  $m/z$  44 and associated ion fragments (e.g.  $m/z$  16, 17, and 18) was also observed for octane and decane SOA.

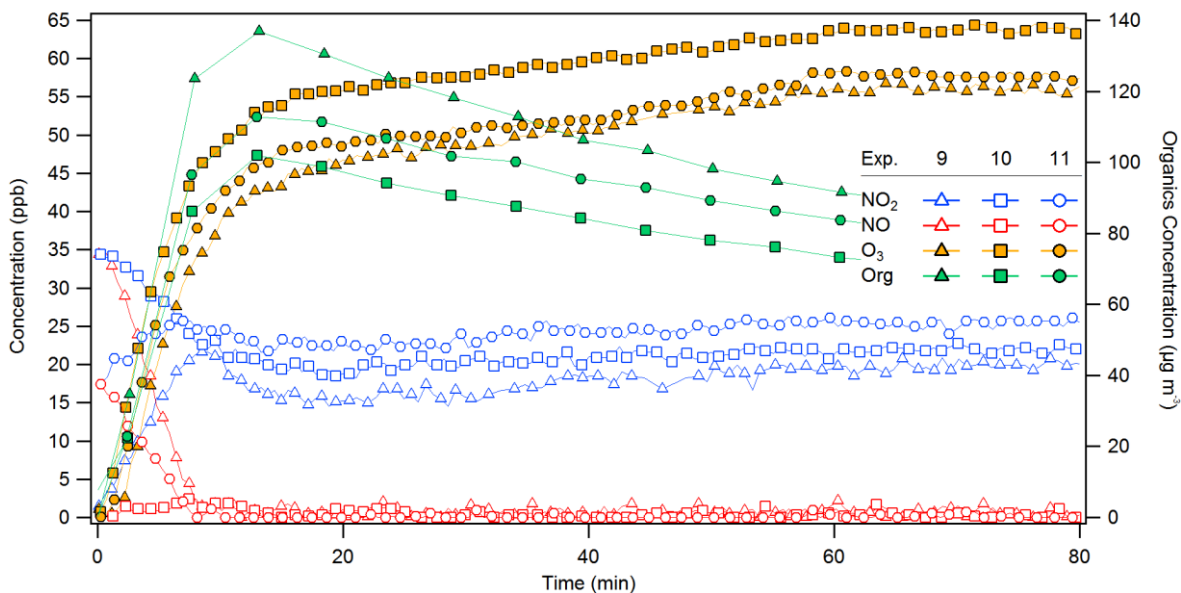


**Figure S2:** Example of NO, NO<sub>2</sub>, O<sub>3</sub> and SOA trends under different starting NO<sub>x</sub> conditions. Exp. 9 (high initial NO), 10 (high initial NO<sub>2</sub>), and 11 (balanced initial NO and NO<sub>2</sub>) for chlorine-initiated oxidation of dodecane under low RH conditions are shown. Ozone production slowed down significantly as the NO<sub>x</sub> concentrations plateaued and as the SOA concentrations approached their maxima. By the end of the photooxidation period (60 min), lowest final NO<sub>x</sub> concentrations (consisting of NO<sub>2</sub> and interferences, which may include alkyl nitrates) and highest SOA concentrations were observed for high initial NO concentrations (Exp. 1 for octane, Exp. 5 for decane, and Exp. 9 for dodecane).

5

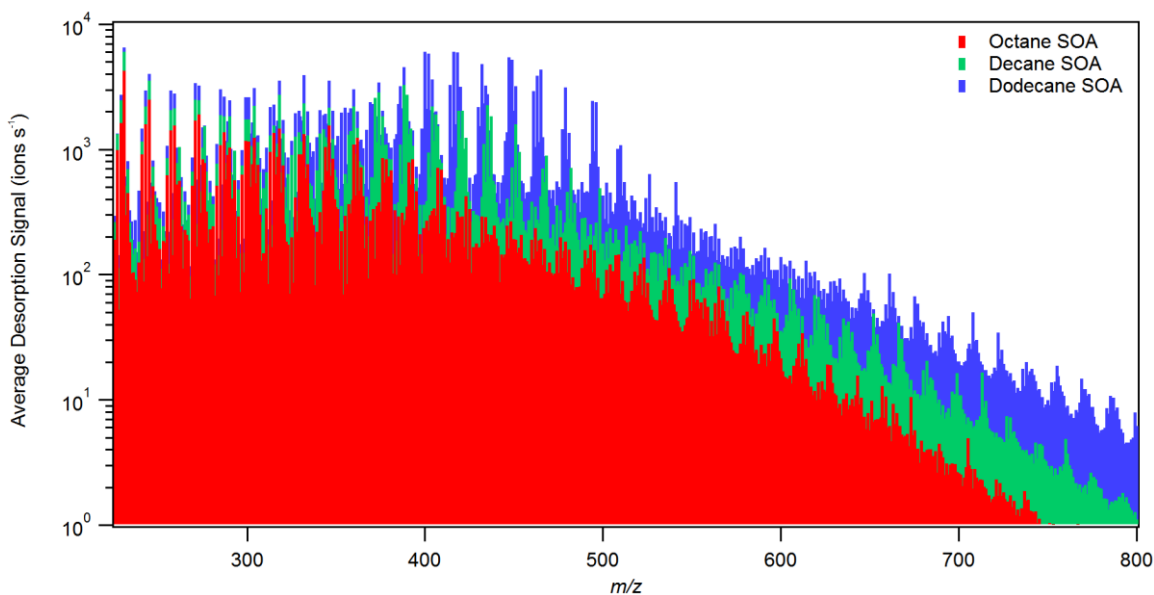
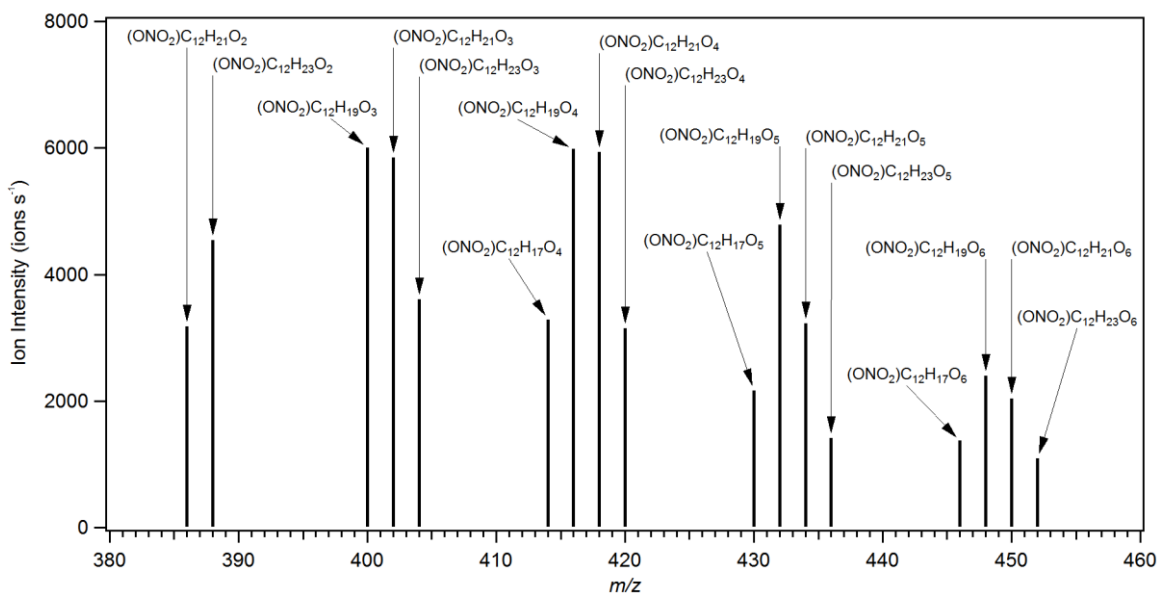


**Figure S3:** Comparison of particle-phase composition during FIGAERO desorption for octane (Exp. 3), decane (Exp. 7), and dodecane (Exp. 11). Same as Figure 4 in the main text but with the y-axis in logarithmic scale and the x-axis ( $m/z$ ) extended to the maximum sampled range. Desorption signals are not stacked.



5

**Figure S4:** Particle-phase distribution of  $C_{12}$  organic (mono-)nitrates. Assuming equal sensitivity, the particle-phase abundance roughly followed a bell-shape distribution across the different oxygenation groups, peaking at the  $O_3$  or  $O_4$  group. Within each oxygenation group, the product distribution follows a bell-shape around  $H_{19}$  and  $H_{21}$  compounds. Similar bell-shaped organic nitrate distribution has been observed for ambient isoprene- and monoterpene-derived organonitrates (Lee et al., 2016).

10

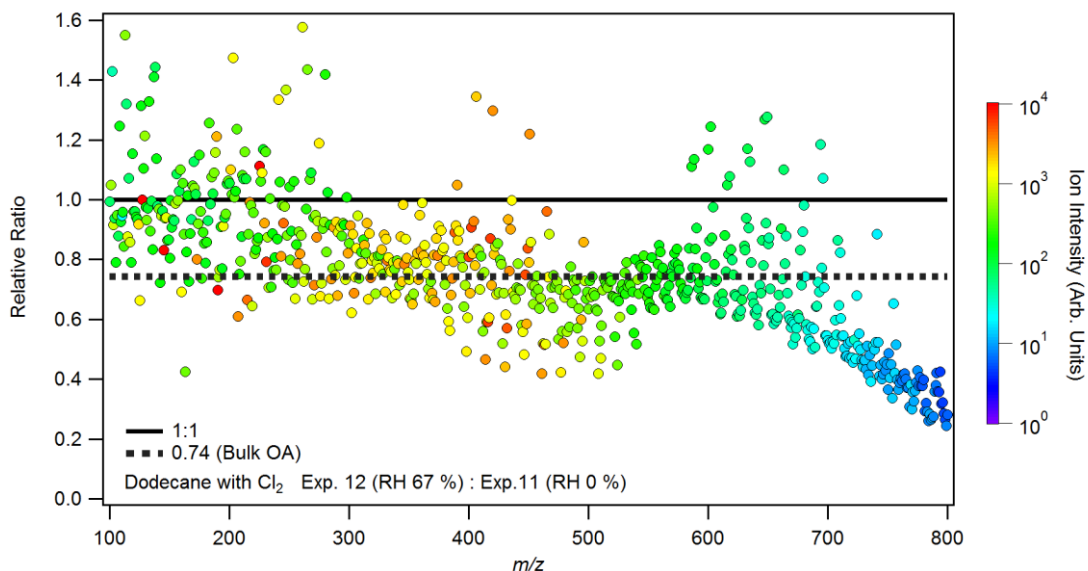


**Figure S5:** Ratio of integrated unit-mass resolution FIGAERO-CIMS desorption signal during temperature ramp from a high-RH SOA formation experiment (Exp. 12, 67 % RH) to that from a low-RH SOA formation experiment (Exp. 11, < 5 % RH). Integrated ion intensity is shown on a logarithmic scale as the color. The ratio of bulk organics concentration during the filter collection period calculated using ACSM data is shown as the dotted black line. Except for the low molecular weight thermal fragmentation/decomposition products and the high molecular weight, low-volatility compounds, the unit-mass ion ratios appear in agreement with bulk measurement. Under high RH conditions, the higher molecular weight ( $m/z > 600$ ) compounds become increasingly suppressed.

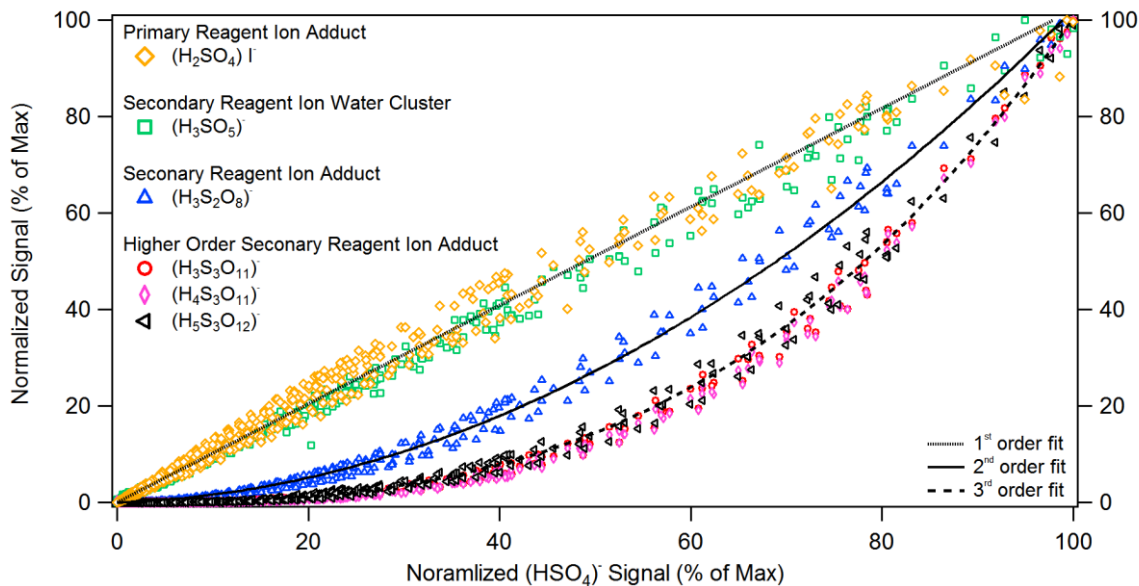


**Figure S6:** Example of secondary  $\text{HSO}_4^-$  ionization products. Ion signals observed during  $(\text{NH}_4)_2\text{SO}_4$  thermal decomposition were first normalized by  $\text{I}^-$  signal and then normalized against the maximum desorption signal observed for each ion. Linear (1<sup>st</sup> order), quadratic (2<sup>nd</sup> order), and cubic equations (3<sup>rd</sup> order) are fitted.

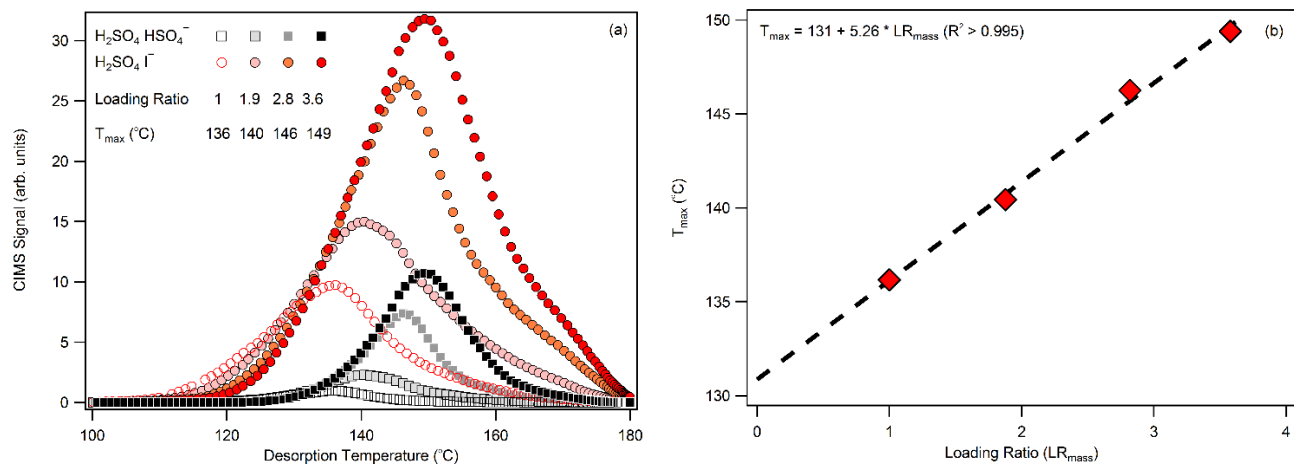


**Figure S7:** The 1-D thermograms for two (NH<sub>4</sub>)<sub>2</sub>SO<sub>4</sub> decomposition product ions. H<sub>2</sub>SO<sub>4</sub>•I<sup>-</sup> was the primary adduct and H<sub>2</sub>SO<sub>4</sub>•HSO<sub>4</sub><sup>-</sup> was a secondary ionization product. The lowest time-integrated desorption ion intensity for H<sub>2</sub>SO<sub>4</sub>•I<sup>-</sup> was used as the basis for calculating the loading ratio (LR<sub>mass</sub>). The loading ratio for H<sub>2</sub>SO<sub>4</sub>•HSO<sub>4</sub><sup>-</sup> (not shown) is the square of that for H<sub>2</sub>SO<sub>4</sub>•I<sup>-</sup> (b) Linear regression fitting of T<sub>max</sub> as a function of the LR<sub>mass</sub>. T<sub>max</sub> increased linearly with mass loading of (NH<sub>4</sub>)<sub>2</sub>SO<sub>4</sub>.

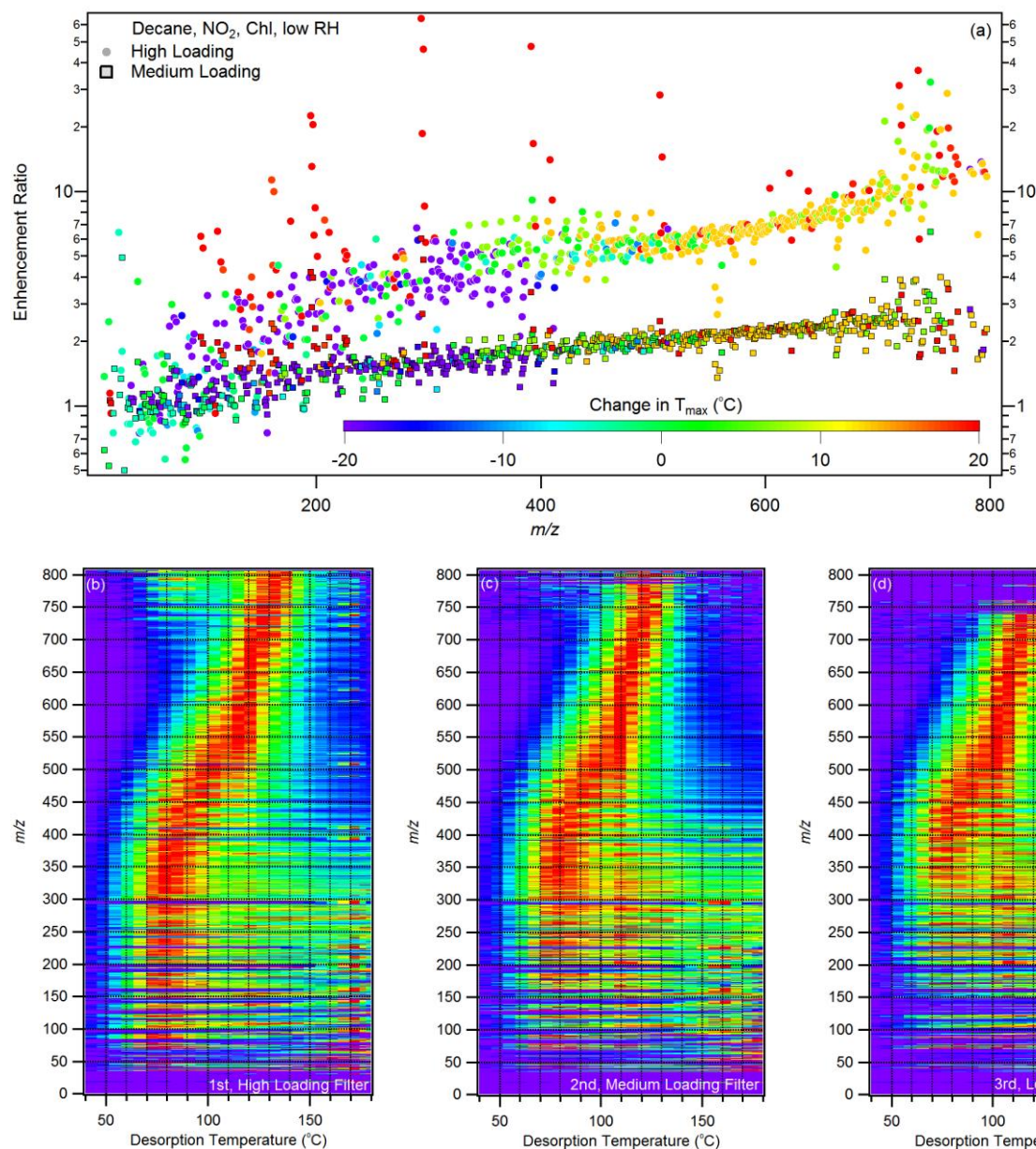


**Figure S8:** Effects of aerosol loading on  $T_{max}$ . Three SOA filter samples were collected during Exp. 6 for 45 mins, 30 mins, and 15 mins, in that order. Each filter was subjected to two full desorption runs to minimize carry-over effects and to determine the filter background. (a) Enhancement ratios calculated using unit-mass integrated signals for the lowest filter loading run as the referenced condition. Color scale shows  $T_{max}$  shifts in °C, using the  $T_{max}$  values observed in the low loading run as the reference point. (b) 2-D thermogram for the first, high loading filter, (c) for the second, medium loading filter, and for (d) the third, low loading filter. For (b-d), the color scale represents the normalized desorption intensity as a percentage of the maximum, same as in Fig. 5 in the main text. Between the time it took for filter collection and filter desorption, the ion intensity of some high molecular weight, low volatility compounds had decreased to below the limits of detection (i.e.  $3\sigma$  of the background signal) in the particle phase, likely due to volatility-dependent wall loss. Disappearance of low  $m/z$  ( $< 300$ ) compounds maybe due to decreases in suspended aerosol concentration, making it unfavorable for semi-volatile compounds to partition to the particle phase, or may be associated with the loss of high molecular weight oligomers, assuming that the low  $m/z$  desorption ions were dominated by low-temperature ( $T_{max} < \sim 80$  °C) thermal fragmentation products as opposed to semi-volatile monomers.

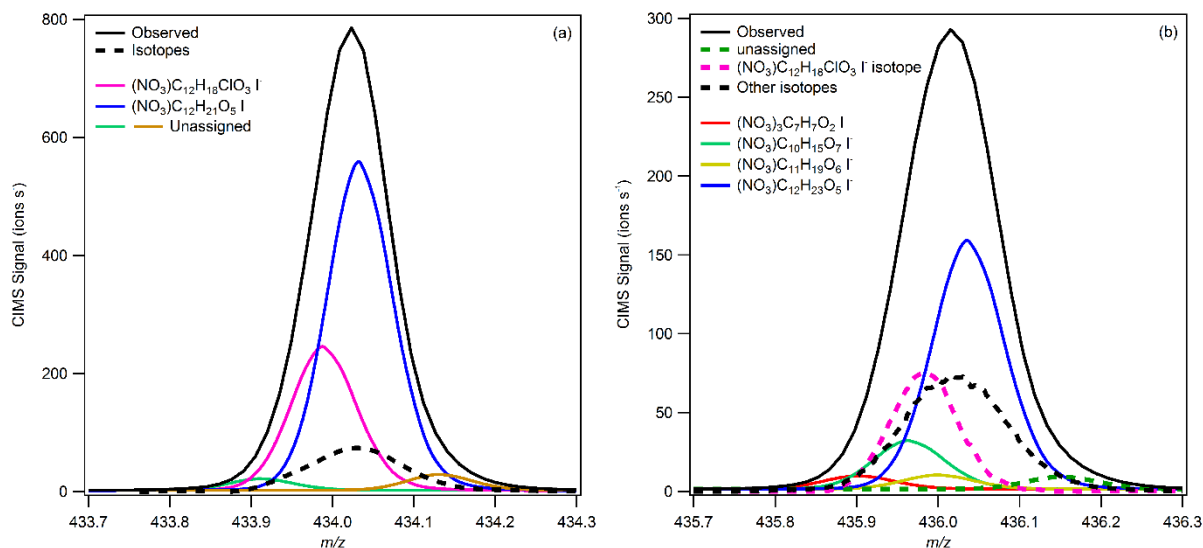


**Figure S9:** High resolution fitting at  $m/z$  (a) 434 and (b) 436 for FIGAERO-CIMS data from Exp. 11. The  $C_{12}$  chloronitrate ( $ONO_2-C_{12}H_{18}ClO_3 \cdot I$ ) peak is tentatively identified in (a) but it overlaps with the nearby stronger organonitrate ( $ONO_2-C_{12}H_{21}O_5 \cdot I$ ) peak. Because the chloronitrate peak is a weaker peak with significant overlap with a stronger peak, quantitative assessment would be challenging due to peak fitting uncertainties (Cubison and Jimenez, 2015). The presence of chloronitrate cannot be confirmed or rejected based on its unique isotopic signature at  $m/z+2$  positions, as shown in (b), where nonchlorinated compounds also dominate.

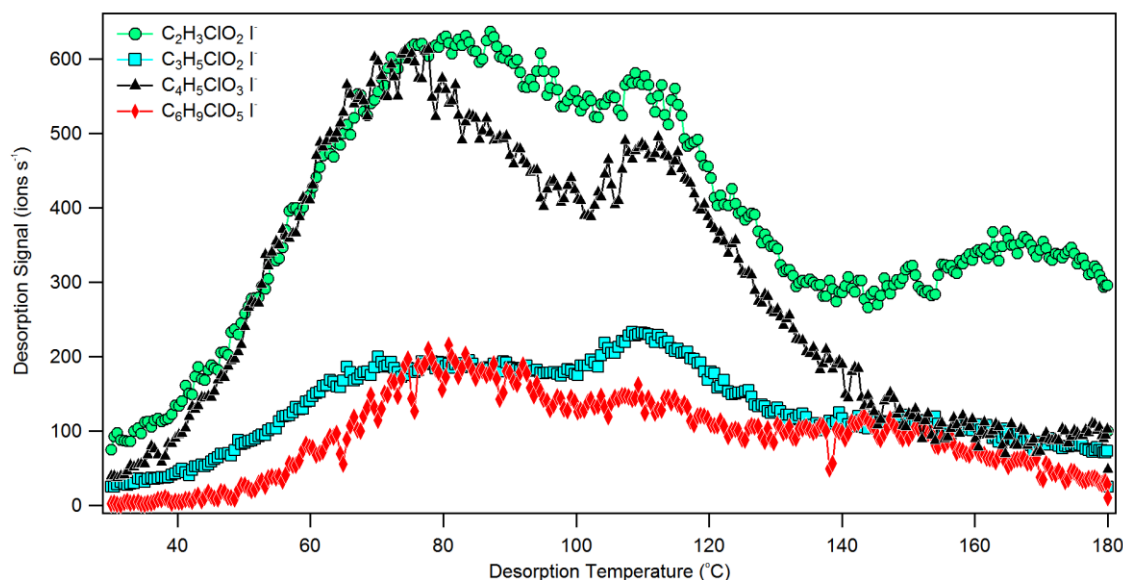


**Figure S10:** 1-D thermogram of select organochlorides observed for Exp 10. All compounds shown exhibited multimodal desorption behaviors.  $C_2H_3ClO_2$  is too volatile to be present as a molecular compound in the particle phase and is therefore a thermal decomposition product.  $C_2H_3ClO_2$  shows three local maxima at  $\sim 87^\circ C$ ,  $\sim 109^\circ C$ , and  $\sim 167^\circ C$ . The  $T_{max}$  for the least volatile desorption mode of  $C_2H_3ClO_2$  is higher than that for ammonium sulfate seed particles ( $\sim 155^\circ C$ ) from the same filter run, and may be produced from thermal decomposition of extremely low volatility organochlorides. However, larger organochloride ions were not observed to have any distinct  $T_{max}$  modes over these very high temperature ranges ( $> 160^\circ C$ )

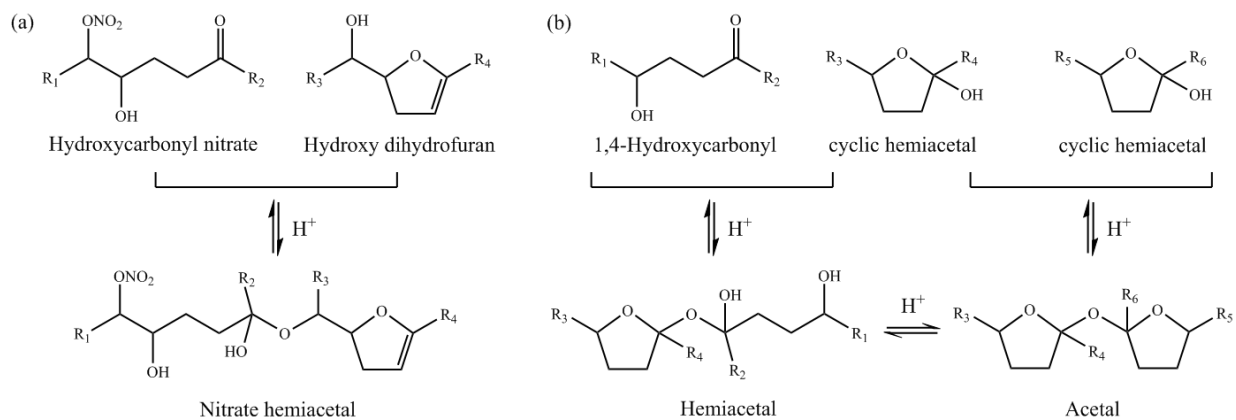


**Figure S11:** Oligomerization via the reaction between (a) carbonyl hydroxyl nitrate and hydroxy dihydrofuran proposed by Schilling Fahnstock et al. (2015) and (b) cyclic hemiacetal with either a 1,4-hydroxycarbonyl or another cyclic hemiacetal proposed by Aimanant and Ziemann (2013). Condensed-phase isomerization between acetal and hemiacetal dimers is also possible, as shown in (b).

## S2. Interaction between Cl, NO<sub>x</sub>, and HO<sub>x</sub>

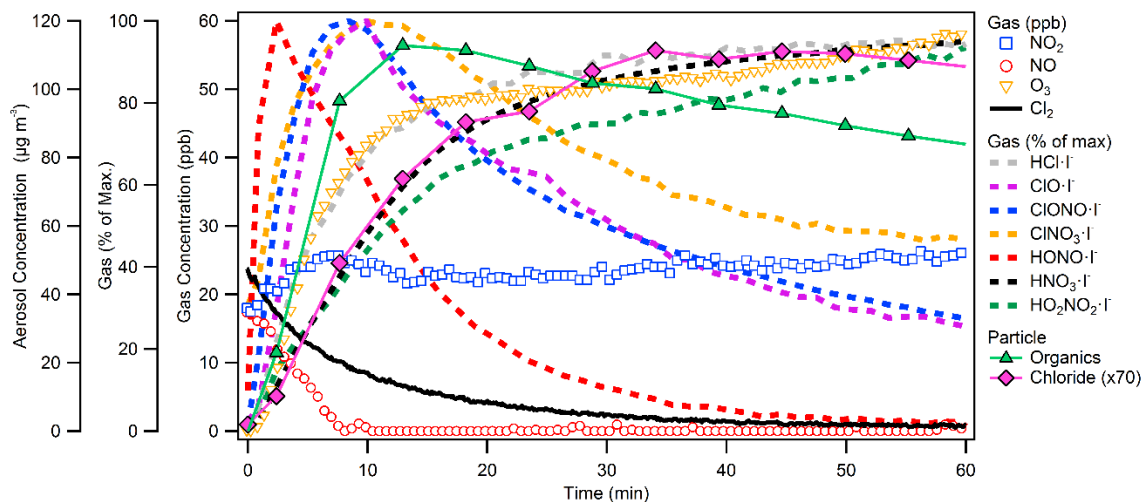
Formation of HO<sub>2</sub>NO<sub>2</sub> likely proceeds via



5 Formation of HONO under UV can proceed via



The trends for HO<sub>2</sub>NO<sub>2</sub>, HONO, and select gas-phase species observed by the I<sup>-</sup> CIMS are shown in Fig. S12.



10 **Figure S12:** Representative trends of SOA and trace gas species during the photooxidation period. Data from dodecane oxidation (Exp. 11) are shown, similar to Fig. 1 in the main text. Additional species shown include ClONO<sub>2</sub> (from reaction between ClONO with NO<sub>2</sub>, Lesar et al., 2006), ClO (possibly a ion fragment of ClONO), HCl (from H-abstraction by Cl<sup>•</sup> or perhaps Cl-elimination reactions), and HNO<sub>3</sub> (due to the oxidation of NO<sub>2</sub> by OH).

## S3. Calculation of Bulk SOA Properties using the FIGAERO-CIMS

15 If equal sensitivity is assumed for all ions (i.e. I<sup>-</sup> adducts detected by the FIGAERO-CIMS), the average molecular weight,  $mw_{avg}$  is estimated based on the (desorption) intensity  $I_i$  and the molecular weight,  $mw_i$  of all ions identified,

$$mw_{avg}(T_d) = \frac{\sum_i mw_i \times I_i(T_d)}{\sum_i I_i(T_d)} \quad \text{Eq. (S1)}$$

where  $mw_{avg}$  and  $I_i$  vary with desorption temperature,  $T_d$  during a single FIGAERO desorption. A single average molecular weight for the entire FIGAERO desorption run can be calculated based on the integrated values over the  $T_d$  range,

20 
$$mw_{SOA} = \frac{\int (\sum_i mw_i \times I_i(T_d)) \Delta T_d}{\int (\sum_i I_i(T_d)) \Delta T_d} \quad \text{Eq. (S2)}$$

where  $\Delta T_d$  is the step change in desorption temperature. It should be noted that because of thermal decomposition, which has also been observed for monomers (Stark et al., 2017), the  $mw_{avg}$  and  $mw_{SOA}$  calculated using the FIGAERO-CIMS data likely underestimate the actual average SOA molecular weight. For octane SOA,  $mw_{SOA}$  calculated in this way ranges from 206 to

226 g mol<sup>-1</sup>; for decane SOA, mw<sub>SOA</sub> ranges from 241 to 265 g mol<sup>-1</sup>; for dodecane SOA, mw<sub>SOA</sub> ranges from 260 to 270 g mol<sup>-1</sup>. The molar SOA yield can then be calculated as,

$$Y_{molar} = \frac{n_{SOA}}{\Delta n_{VOC}} = \frac{m_{SOA}/mw_{SOA}}{\Delta m_{VOC}/mw_{VOC}} = Y \frac{mw_{VOC}}{mw_{SOA}} \quad \text{Eq. (S3)}$$

where n<sub>SOA</sub> and n<sub>VOC</sub> are the molar concentrations of SOA and VOC. The molecular weight of VOC, mw<sub>VOC</sub> is known for the alkane precursors. The corresponding molar yield ranges from 0.08 to 0.14 for octane SOA, 0.26 to 0.47 for decane SOA, and 0.72 to 1.04 for dodecane SOA. The above-unity molar SOA yield observed for dodecane (Exp. 9) indicates that SOA mass may be overestimated, which may be the result of uncertainties with the collection efficiency (CE) and relative ionization efficiency (RIE) assumed for the SOA.

Equations S1 and S2 can also be used to calculate various other bulk SOA properties, including elemental ratios such as the oxygen-to-carbon ratio (O:C), hydrogen-to-carbon ratio (H:C), nitrate-to-carbon ratio (NO<sub>3</sub>:C), chloride-to-carbon ratio (Cl:C), or the oxidation state of carbon (OS<sub>C</sub>). Using the oxygen-to-carbon ratio (O:C) as the example, the bulk SOA elemental ratios as a function of the FIGAERO desorption temperature, T<sub>d</sub> can be calculated as

$$O:C_{avg}(T_d) = \frac{n_O(T_d)}{n_C(T_d)} = \frac{\sum_i n_{O,i} \times I_i(T_d)}{\sum_i n_{C,i} \times I_i(T_d)} \quad \text{Eq. (S4)}$$

where n<sub>O</sub> is the total number of oxygen atoms present in the desorbed ions at T<sub>d</sub>, n<sub>C</sub> is the total number of carbon atoms, n<sub>O,i</sub> is the number of oxygen atom present in compound *i* as determined by its assigned molecular formula (which is independent of T<sub>d</sub>), n<sub>C,i</sub> is the number of carbon present in compound *i*, and I<sub>i</sub> is the desorption ion intensity for compound *i* at T<sub>d</sub>. Equal sensitivity is assume for ions used for the analysis such that I<sub>i</sub> can be used as the molar amount for compound *i*.

## References

- Aimanant, S. and Ziemann, P. J.: Chemical mechanisms of aging of aerosol formed from the reaction of n-pentadecane with OH radicals in the presence of NO<sub>x</sub>, *Aerosol Sci. Technol.*, 47(9), 979–990, doi:10.1080/02786826.2013.804621, 2013.
- 5 Cubison, M. J. and Jimenez, J. L.: Statistical precision of the intensities retrieved from constrained fitting of overlapping peaks in high-resolution mass spectra, *Atmos. Meas. Tech.*, 8(6), 2333–2345, doi:10.5194/amt-8-2333-2015, 2015.
- Hu, W., Campuzano-Jost, P., Day, D. A., Croteau, P., Canagaratna, M. R., Jayne, J. T., Worsnop, D. R. and Jimenez, J. L.: Evaluation of the new capture vaporizer for aerosol mass spectrometers (AMS) through field studies of inorganic species, *Aerosol Sci. Technol.*, 51(6), 735–754, doi:10.1080/02786826.2017.1296104, 2017.
- 10 Lee, B. H., Mohr, C., Lopez-Hilfiker, F. D., Lutz, A., Hallquist, M., Lee, L., Romer, P., Cohen, R. C., Iyer, S., Kurtén, T., Hu, W., Day, D. A., Campuzano-Jost, P., Jimenez, J. L., Xu, L., Ng, N. L., Guo, H., Weber, R. J., Wild, R. J., Brown, S. S., Koss, A., de Gouw, J., Olson, K., Goldstein, A. H., Seco, R., Kim, S., McAvey, K., Shepson, P. B., Starn, T., Baumann, K., Edgerton, E. S., Liu, J., Shilling, J. E., Miller, D. O., Brune, W., Schobesberger, S., D’Ambro, E. L. and Thornton, J. A.: Highly functionalized organic nitrates in the southeast United States: Contribution to secondary organic aerosol and reactive nitrogen budgets, *Proc. Natl. Acad. Sci.*, 113(6), 201508108, doi:10.1073/pnas.1508108113, 2016.
- 15 Lesar, A., Kovačič, S. and Hodošček, M.: ClONO and BrONO loss mechanisms in the presence of NO<sub>2</sub>: A quantum-mechanical study, *Chem. Phys. Lett.*, 429(4–6), 343–349, doi:10.1016/j.cplett.2006.07.058, 2006.
- Lim, Y. B. and Ziemann, P. J.: Effects of molecular structure on aerosol yields from OH radical-initiated reactions of linear, branched, and cyclic alkanes in the presence of NO<sub>x</sub>, *Environ. Sci. Technol.*, 43(7), 2328–2334, doi:10.1021/es803389s, 2009.
- 20 Ng, N. L., Canagaratna, M. R., Jimenez, J. L., Zhang, Q., Ulbrich, I. M. and Worsnop, D. R.: Real-time methods for estimating organic component mass concentrations from aerosol mass spectrometer data, *Environ. Sci. Technol.*, 45(3), 910–916, doi:10.1021/es102951k, 2011.
- Schilling Fahnstock, K. A., Yee, L. D., Loza, C. L., Coggon, M. M., Schwantes, R., Zhang, X., Dalleska, N. F. and Seinfeld, J. H.: Secondary Organic Aerosol Composition from C<sub>12</sub> Alkanes, *J. Phys. Chem. A*, 119(19), 4281–4297, doi:10.1021/jp501779w, 2015.
- 25 Stark, H., Yatavelli, R. L. N., Thompson, S. L., Kang, H., Krechmer, J. E., Kimmel, J. R., Palm, B. B., Hu, W., Hayes, P. L., Day, D. A., Campuzano-Jost, P., Canagaratna, M. R., Jayne, J. T., Worsnop, D. R. and Jimenez, J. L.: Impact of Thermal Decomposition on Thermal Desorption Instruments: Advantage of Thermogram Analysis for Quantifying Volatility Distributions of Organic Species, *Environ. Sci. Technol.*, 51(15), 8491–8500, doi:10.1021/acs.est.7b00160, 2017.
- 30 Ulbrich, I. M., Canagaratna, M. R., Zhang, Q., Worsnop, D. R. and Jimenez, J. L.: Interpretation of Organic Components from Positive Matrix Factorization of Aerosol Mass Spectrometric Data., *Atmos. Chem. Phys.*, 9, 2891, doi:10.5194/acp-9-

2891-2009, 2009.

Wang, D. S. and Hildebrandt Ruiz, L.: Secondary organic aerosol from chlorine-initiated oxidation of isoprene, *Atmos. Chem. Phys.*, 17(22), 13491–13508, doi:10.5194/acp-17-13491-2017, 2017.